Journal of Soils and Sediments (2021) 21:3933–3947
https://doi.org/10.1007/s11368-021-03054-2

SEDIMENTS, SEC 3 • HILLSLOPE AND RIVER BASIN SEDIMENT DYNAMICS • RESEARCH ARTICLE

Variability of extreme precipitation and rainfall erosivity and their attenuated effects on sediment delivery from 1957 to 2018 on the Chinese Loess Plateau

Xiaoming Xu[1] · Du Lyu[2] · Xiangjie Lei[3] · Tao Huang[1] · Yali Li[4] · Haijie Yi[2] · Jinwei Guo[5] · Liang He[1] · Jie He[1] · Xihua Yang[6] · Mancai Guo[7] · Baoyuan Liu[1] · Xiaoping Zhang[1,2]

Received: 22 February 2021 / Accepted: 10 August 2021 / Published online: 24 August 2021
© The Author(s), under exclusive licence to Springer-Verlag GmbH Germany, part of Springer Nature 2021

Abstract

Purpose The Chinese Loess Plateau, characterized by severe soil erosion and a vulnerable environment, is highly sensitive to extreme weather events. Understanding the changing patterns of extreme precipitation events and the associated rainfall erosivity, as well as their effects on the soil erosion and sediment delivery, is essential to the application of planning and ecological restoration on the Loess Plateau.

Materials and methods In total, 100 meteorological stations with high-quality daily data spanning from 1957 to 2018 were used to extract eight indices to evaluate the variations in extreme precipitation and the associated rainfall erosivity, and to identify the contribution of extreme precipitation to rainfall erosivity and thus to sediment delivery.

Results and discussion The annual extreme precipitation from six of eight indices all exhibited insignificant decreases in the study area. The average annual rainfall erosivity was 1159 MJ mm ha^{-1} h^{-1} $year^{-1}$, with a slight decreasing rate of − 3.16 MJ mm ha^{-1} h^{-1} $year^{-1}$ over a 10-year period. The rainfall erosivity presented a staged descending change ranging from the 1960s to the late 1990s, but a promptly ascending change since 2000. These variations in extreme precipitation and the associated rainfall erosivity in the region were very likely to be affected by the changing pattern of the East Asian summer monsoon. The annual precipitation from three kinds of extreme events, namely, maximum 5-day precipitation (RX5d), heavy precipitation (R20), and very wet day precipitation (R95p), contributed 60–90% of the annual rainfall erosivity, respectively. Compared with the reference period (1957–1979), the rainfall erosivity resulting from extreme precipitation events contributed less to the dramatic reduction in sediment delivery on the Loess Plateau in the periods of 1980 to 1999 and 2000 to 2018.

Conclusions The results imply a reduced impact of rainfall erosivity and increased human intervention on sediment delivery on the Loess Plateau in the last 60 years. These findings are useful in understanding the processes of ecohydrology and soil erosion delivery in the region.

Keywords Spatiotemporal variations · Rainfall erosivity · Extreme precipitation · Sediment delivery · Loess Plateau

Responsible editor: Paolo Porto

✉ Xiaoping Zhang
zhangxp@ms.iswc.ac.cn

[1] Institute of Soil and Water Conservation, Northwest A&F University, Yangling 712100, Shaanxi, China

[2] Institute of Soil and Water Conservation, Chinese Academy of Science and Ministry of Water Resources, Yangling 712100, Shaanxi, China

[3] Climate Center of Shaanxi Province, Xi'an 710015, China

[4] Meteorological Information Center of Shaanxi Province, Xi'an 710015, China

[5] College of Natural Resources and Environment, Northwest A&F University, Yangling 712100, China

[6] Department of Planning, Industry and Environment, PO Box 644, Parramatta, NSW 2124, Australia

[7] Faculty of Science, Northwest A&F University, Yangling 712100, Shaanxi, China

1 Introduction

Soil erosion has caused serious land resource degradation and brought extensive concern about the eco-environment worldwide (Panagos et al. 2015). Wischmeier and Smith (1978) and Renard et al. (1997) defined rainfall erosivity (R) as the potential ability to cause soil erosion in the Universal Soil Loss Equation, and R is also included in the Chinese Soil Loss Equation (Liu et al. 2002). As a key factor, R reflects the influence of rainfall amount, duration, intensity, and kinetic energy on soil erosion especially in extreme precipitation events (Hoyos et al. 2005; Ballabio et al. 2017).

China's Loess Plateau is considered to be one of the most vulnerable areas worldwide and delivers large amounts of sediment to the Yellow River (Tang et al. 1993; Cai 2001). Due to the highly fragmented terrain, steep slopes, low vegetation cover, erodible soil, and long history in farming, the Loess Plateau is very sensitive to several extreme precipitation events and their changes (Zhang et al. 2018).

Many studies have focused on extreme precipitation events, rainfall erosivity, and sediment change on the Loess Plateau. Zhou et al. (1992) reported that heavy precipitation events with a high intensity and short duration contributed to approximately 90% of the annual total soil erosion in this region. Li et al. (2010) selected several typical extreme precipitation indices and found that most indices showed an obvious changing gradient from low latitudes to high latitudes on the Loess Plateau; however, there was no significant change from 1961 to 2007. Sun et al. (2016) showed that the numbers of days of erosive precipitation (R12), heavy precipitation (R20), rainstorms (R50), and maximum 5-day precipitation (RX5d) exhibited insignificant variations on the Loess Plateau during 1960–2013.

Regarding R, Xin et al. (2011) illustrated that R had a remarkable spatial difference and decreased significantly in the period from 1956 to 2008 on the Loess Plateau. Yang and Lu (2015) detected a slight decrease in R on the wetter eastern side of the Northwest China covering the Loess Plateau. Liu et al. (2018) revealed that Jinghe Basin, a typically vulnerable area on the hinterland of the Loess Plateau, exhibited an evident spatial pattern in R and a significant positive correlation between annual precipitation and R.

According to Liu et al. (2019), the sediment load in the Yellow River has declined by approximately 90% in the last 20 years compared to that before 1980. Liu et al. (2016) reported that rainstorms (R50) contributed approximately 40–50% of the total annual sediment yield generated from a region with severe soil loss region on the Loess Plateau, but the effects of precipitation events of 10–50 mm per day on sediment yield could not be ignored in this region. Wang et al. (2016) showed that human activities such as soil and water conservation measures and vegetation restoration have decreased sediment yield from the heartland of Loess Plateau by 53% in 1980–1999 and 57% in 2000–2010, respectively.

It is well known that soil erosion is caused by a few extreme precipitation events over China's Loess Plateau (Zhou et al. 1992; Wei et al. 2007; Ran et al. 2012; Vallebona et al. 2015; Zhao et al. 2018). However, it is not very clear about what the changing pattern of the extreme precipitation events under global climate change is, what their different contributions to R are, how they change, and how these changes affect sediment yield. Therefore, the objectives of the work were to (1) examine the spatiotemporal changes in extreme precipitation events and R over the Loess Plateau in the past 62 years; (2) identify the contribution of extreme precipitation events to R based on extreme precipitation indices; and (3) quantify the effect of extreme precipitation events and associated R on sediment yield on the Loess Plateau in different time periods. The findings from this study will help to understand the variability of extreme precipitation events under the background of global climate change and the soil erosion processes and sediment delivery that occur on the Loess Plateau.

2 Data source and methods

2.1 Study area

As the largest loess accumulation region on Earth, the Loess Plateau is bounded by 100.8°–114.6°E and 33.7°–41.3°N, covering a total area of approximately 6.24×10^5 km^2. Most parts of the plateau range from 400 to 3000 m a.s.l. The zonal soil is mainly cambisol and lixisol in the World Reference Base for Soil Resources and the average loess thickness is 100–200 m (Tang et al. 1993). The mean annual precipitation of the Loess Plateau is approximately 440 mm and it contains several climate zones from sub-humid in the southeast to arid in the northwest (Fig. 1). The vegetation correspondingly shows obvious zonal changes from forest to desert steppe.

The fluctuation of the East Asian summer monsoon predominantly affects the climate characteristics of this region. Precipitation is unevenly distributed annually and seasonally. Approximately 70–80% of the precipitation is concentrated in summer and autumn. Extreme precipitation events and correspondingly high R often lead to serious soil erosion as well as drought disasters in this region. The Loess Plateau accounts for more than approximately 90% of the sediment of the Yellow River (Wang et al. 2016). Engineering measures including terraces, reservoirs, and check dams constituted the main soil conservation measures used prior to 1999 (Chen et al. 2007). Vegetation restoration has been carried out by the Chinese government since 1999. The total vegetation coverage was estimated to have improved significantly

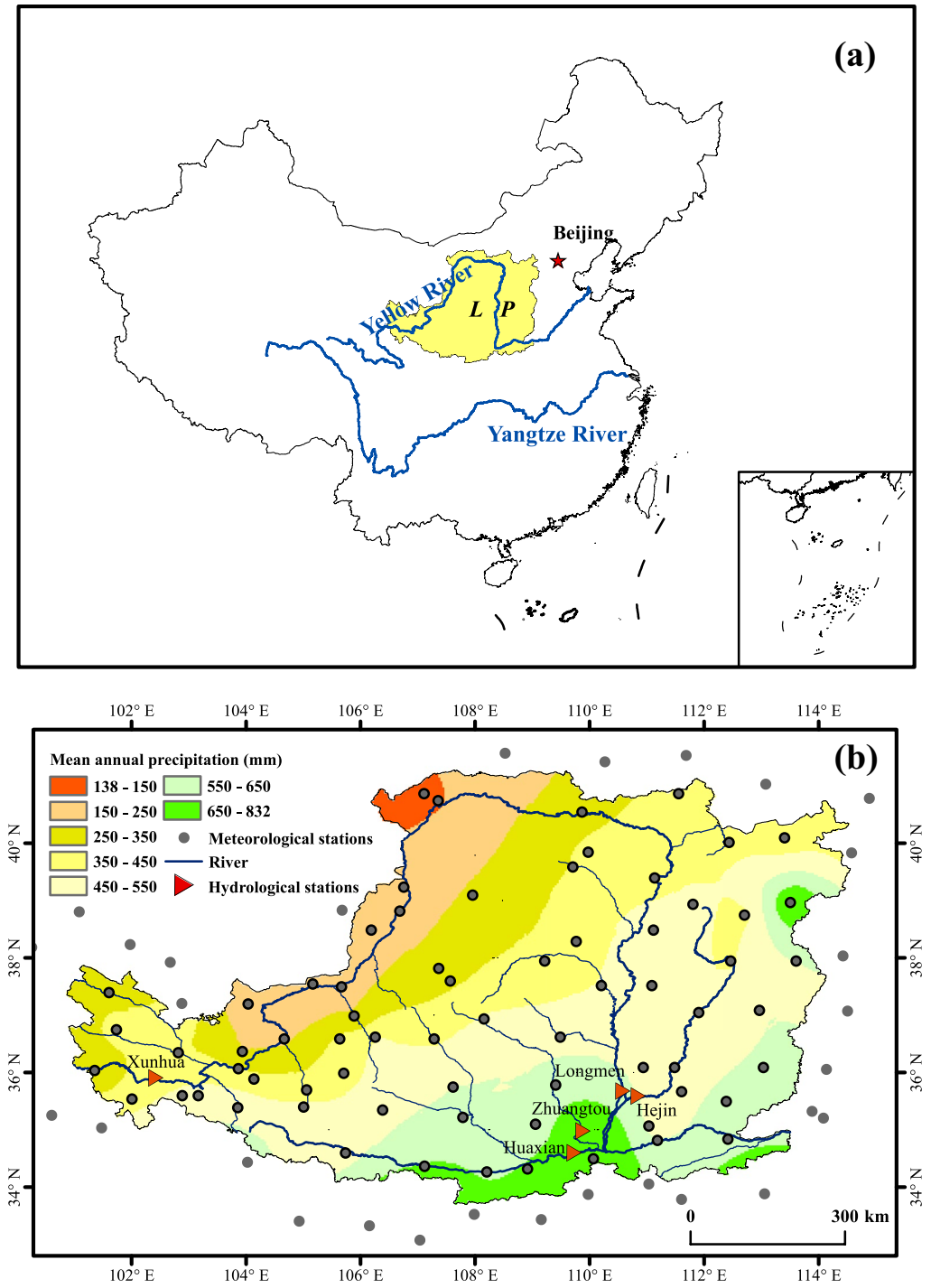

Fig. 1 The location of the Loess Plateau in China (**a**), the distribution of meteorological stations on and around the Loess Plateau, and the spatial distribution of mean annual precipitation across the Loess Plateau for the period 1957 to 2018 (**b**). The red triangles denote the hydrological stations (including Xunhua, Hejin, Longmen, Huaxian, and Zhuangtou) in the main channel of the Yellow River and the primary tributaries from which sediment delivery from the Loess Plateau was derived

across the Loess Plateau, from about 40 in 1982 to 76.8% in 2017 (Li et al. 2019; Yang et al. 2020). The area with soil loss was estimated to have reduced from 4.3×10^5 km^2 in the early 1980s to 2.14×10^5 km^2 in 2018 on the Loess Plateau (Ministry of Water Resources of the People's Republic of China 2019).

2.2 Data and processing

A total of 100 meteorological observation stations were evenly distributed in and around the Loess Plateau (Fig. 1). Daily precipitation data for the period 1957–2018 were gathered from the China Meteorological Data Sharing Network (http://data.cma.cn/). We implemented thorough quality control and consistency checks for data to ensure reliability.

We adopted the commonly used erosive rainfall criterion in China (daily precipitation greater than 12 mm) (Wischmeier and Smith 1978) in this study. We chose eight extreme precipitation indices in this study based on recommendations from the FAO when they worked on climate change detection (Table 1). The R of this region in the past 62 years was calculated based on a daily scale and then summed to monthly and annual intervals. Following the idea proposed by Liu et al. (2019), the amount of sediment delivered from the Loess Plateau was approximated from the difference between the sum at four hydrological stations (i.e., Hejin, Longmen, Huaxian, and Zhuangtou) near the outlet of the Loess Plateau and that at the Xunhua gauge station at the entrance of the Plateau. The annual sediment delivery data at these stations during 1957–2018 were obtained from Liu et al. (2019).

The East Asian summer monsoon index (EASMI) refers to an area-averaged summer (June to August) dynamical normalized seasonality (DNS) at 850 hPa within the East Asian monsoon domain (10°–40°N, 110°–140°E) (Li and Zeng 2002). Li and Zeng (2002) and Yin et al. (2019) found periodicity in the annual variation in the EASMI during the periods before 1979, from 1980 to 1999, and after 1999. Additionally, the change points of 1979 and 1999 were always used to divide the time periods to investigate the trends of streamflow and sediment load in most of the research on the Loess Plateau (Zhao et al. 2013; Wang et al. 2016; Zhang et al. 2018). Three time periods, namely, 1957–1979, 1980–1999, and 2000–2018, were therefore used here to examine the variability of extreme precipitation and the associated R as well as their effects on sediment delivery in different periods.

2.3 Methods

2.3.1 Rainfall erosivity estimation

The R was estimated from daily rainfall as proposed by Xie et al. (2016). It was proven that the accuracy of the R factor was much higher when the seasonality was considered (Richardson et al. 1983). The formulas are as follows:

$$\overline{R} = \sum_{k=1}^{24} \overline{R}_{\text{half- month k}} \tag{1}$$

$$\overline{R}_{\text{half- month k}} = \frac{1}{N} \sum_{\text{i}=1}^{N} \sum_{j=0}^{m} \left(\alpha \cdot P_{i,j,k}^{1.7265} \right) \tag{2}$$

$$\overline{WR}_{\text{half - month k}} = \frac{\overline{R}_{\text{half - month k}}}{\overline{R}} \tag{3}$$

where $\overline{R}$ indicates the mean annual rainfall erosivity (MJ mm ha^{-1} h^{-1} year^{-1}); k = 1,2….., 24, which means 24-half months in a year; $R_{\text{half month k}}$ is the rainfall erosivity estimated for the k-th half month (MJ mm ha^{-1} h^{-1} year^{-1}); i = 1,2……, N, which represents the time nodes 1957–2018; j = 0,……, m, where m denotes the days with erosive precipitation in a half month in year i (days of erosive precipitation refers to daily precipitation ≥ 12 mm); and $P_{i,j,k}$ is the total erosive daily precipitation (mm) on the j-th day in the k-th half month of year i. When no erosive precipitation occurred in a certain half month of a year, i.e., j = 0, then $P_{i,j,k} = 0$; a is a parameter, which has seasonality feature (in the warm season of May–September, α is 0.3937; in the cold season of January–April and October–December, a is 0.3101); and $\overline{\text{WR}}_{\text{half-month}}$ refers to the ratio of the mean rainfall erosivity of the k-th half month ($\overline{R}_{\text{half month k}}$) to the mean annual rainfall erosivity ($\overline{R}$).

Table 1 Indices of extreme precipitation adopted in this work

Index type	Number	Index	Description	Definition	Units
Intensity	1	RX1d	Maximum 1-day precipitation	Annual maximum for 1-day precipitation	mm
	2	RX5d	Maximum 5-day precipitation	Annual maximum for 5-day precipitation	mm
	3	EPI	Erosive precipitation intensity	Mean precipitation for erosive precipitation days	mm/day
Absolute indices	4	R12	Erosive precipitation	Annual total precipitation on condition of Rd ≥ 12 mm	mm
	5	R20	Heavy precipitation	Annual total precipitation on condition of Rd ≥ 20 mm	mm
	6	R50	Rainstorm	Annual total precipitation on condition of Rd ≥ 50 mm	mm
	7	R95p	Very wet day precipitation	Annual total precipitation on condition of Rd > 95th percentile	mm
	8	R99p	Extremely wet day precipitation	Annual total precipitation on condition of Rd > 99th percentile	mm

Rd denotes the daily precipitation

2.3.2 Trend analysis of extreme precipitation and rainfall erosivity

The nonparametric Mann–Kendall (MK) method (Mann 1945; Kendall 1975) is recommended to detect the trends in hydrology and climatology sequences because of its simplicity and robustness in handling missing values and extreme values.

The null hypothesis H_0 represents the observed sample data. x_i ($i = 1,2,3\ldots n$) are independent of each other and identically distributed. The alternative hypothesis H_1 indicates a monotonic trend in x_i. The MK test statistic S is derived as follows:

$$S = \sum_{k=1}^{n-1} \sum_{j=k+1}^{n} \operatorname{sgn}(x_j - x_k) \tag{4}$$

$$\operatorname{sgn}(x_j - x_k) = \begin{cases} 1 & x_j - x_k > 0 \\ 0 & x_j - x_k = 0 \\ -1 & x_j - x_k < 0 \end{cases} \tag{5}$$

where x_j and x_k are the statistical values ($j > k$). n indicates the observation length of the data series and sgn (x_j—x_k) is the return function. For the cases in which $n \geq 10$, the statistic S denotes a normal distribution and E(S) = 0. The variances are calculated based on the following formula:

$$VAR(S) = \frac{1}{18}\left[n(n-1)(2n+5) - \sum_{p=1}^{q} t(t-1)(2t+5)\right] \tag{6}$$

where q and t are the number of tied groups and data values, respectively. The standard test statistic Z is calculated as follows:

$$Z = \begin{cases} \frac{S-1}{\sqrt{VAR(S)}} & \text{if } S > 0 \\ 0 & \text{if } S = 0 \\ \frac{S+1}{\sqrt{VAR(S)}} & \text{if } S < 0 \end{cases} \tag{7}$$

where the statistical value Z possesses the characteristics of a standard normal distribution. H_0 will be rejected under the condition of $|Z| \geq Z_{1-\alpha/2}$ at the level of significance in bilateral trend detection. A positive (negative) Z value denotes an ascending (descending) trend. When $|Z| \geq 1.28$, 1.64, and 2.32, this means that it conforms to the significance tests of 90%, 95%, and 99%, respectively.

The Sen's estimator can be utilized to estimate the slope of detected data under the condition that the meteorological and hydrological elements exhibit a linear trend (Sen 1968). Fortunately, the estimator is insensitive to abnormal values and is capable of accurately calculating the magnitude of a trend in a time series (Yue et al. 2002). The $f(t)$ is as follows:

$$f(t) = Qt + B \tag{8}$$

In Eq. (8), Q indicates the magnitude of the trend, and B denotes a constant. The estimated slope Q of all detected data is calculated using the following formula:

$$Q_i = \frac{x_j - x_k}{j - k}; i = 1, 2, \cdots, N \tag{9}$$

where x_j and x_k denote the data values ($j > k$). If n values of x_k are involved during the study period, then N = n (n-1)/2 slope estimates (Q_i) will be calculated. Sen's slope estimator refers to the median of these N values, and N values of Q_i are arranged in the order of smallest to largest. Q_i is calculated depending on whether N is odd or even, as shown in the following formula:

$$Q_i = \begin{cases} Q_{\frac{N+1}{2}} & \text{if N is odd} \\ \frac{1}{2}\left(Q_{\frac{N}{2}} + Q_{\frac{N+2}{2}}\right) & \text{if N is even} \end{cases} \tag{10}$$

2.3.3 Quantifying the contribution of rainfall erosivity to sediment delivery

In this paper, the double mass curve method (Searcy et al. 1960) was applied to estimate the contribution of R to sediment delivery reduction. The specific details are given in the following formulas:

$$\Delta S_T = \overline{S}_2 - \overline{S}_1 \tag{11}$$

where ΔS_T represents the total change in the mean annual sediment delivery, and $\overline{S}_1$ and $\overline{S}_2$ denote the mean annual sediment delivery in the first period and the second period, respectively.

ΔS_T could be approximated as the sum of the changes in sediment delivery due to climate change (ΔS^{Clim}) and human activities (ΔS^{Hum}), as follows:

$$\Delta S_T = \Delta S^{\mathrm{Clim}} + \Delta S^{Hum} \tag{12}$$

The accumulative rainfall erosivity $\sum R_1$ and the accumulative sediment delivery $\sum S_1$ in the first period were related to establishing a regression expressed as follows:

$$\sum S_1 = k \sum R_1 + b \tag{13}$$

where k and b are regression coefficients.

When the cumulative R of the second period was applied to Eq. (13), the mean annual sediment delivery S'_2 in the second period was then obtained using Eq. (14).

$$\sum S'_2 = k \sum R_2 + b \tag{14}$$

The change in sediment delivery ΔS^{Hum} caused by human activities was then estimated using the following formula:

$$\triangle S^{Hum} = \overline{S}_2' - \overline{S}_2 \quad (15)$$

The contribution of human activities to the reduction of sediment delivery between the two periods was estimated by ($\Delta S^{Hum}/\Delta S_T$), and the remaining value (1-$\Delta S^{Hum}/\Delta S_T$)was attributed to climate change.

3 Results

3.1 Variation in extreme precipitation

Temporally, seven of eight extreme precipitation indices manifested decreasing changes except the intensity of erosive precipitation (EPI), which showed an insignificant increase, while very wet day precipitation (R95p) demonstrated a significant descending trend ($P < 0.05$) over the Loess Plateau from 1957 to 2018 (Fig. 2). R95p evidenced the fastest change rate at − 0.39 mm a^{-1}, and the maximum 1-day precipitation (RX1d) was the slowest at − 0.04 mm a^{-1} (Fig. 2a, f). Erosive precipitation (R12) occurred on an average of 10.41 days on the Loess Plateau (Fig. 2c). The average numbers of days with heavy precipitation (R20) and R95p were 4.63 and 4.85, respectively, which were slightly shorter than the 5 days used in the maximum 5-day precipitation (RX5d) (Fig. 2b, d, and f). We noted that rainstorms (R50) occurred on average once every 2 years on the Loess Plateau (Fig. 2e), while the extremely wet day precipitation (R99p) occurred nearly once a year (Fig. 2g).

Spatially, the area with decreasing changes in RX1d, R12, and R50 was generally greater than that with increasing changes on the Loess Plateau. Correspondingly, 43, 38, and 39 of the 70 stations on the Plateau exhibited a negative change; however, only 1, 2, and 0 stations were statistically significant ($P < 0.1$) (Fig. 3a, c, and e). The areas with decreasing changes in R95p and R99p covered 88.9% and 79% of the total region, respectively (Fig. 3f, g). However, the areas with increasing changes were nearly equal to those with decreasing changes in the extreme precipitation

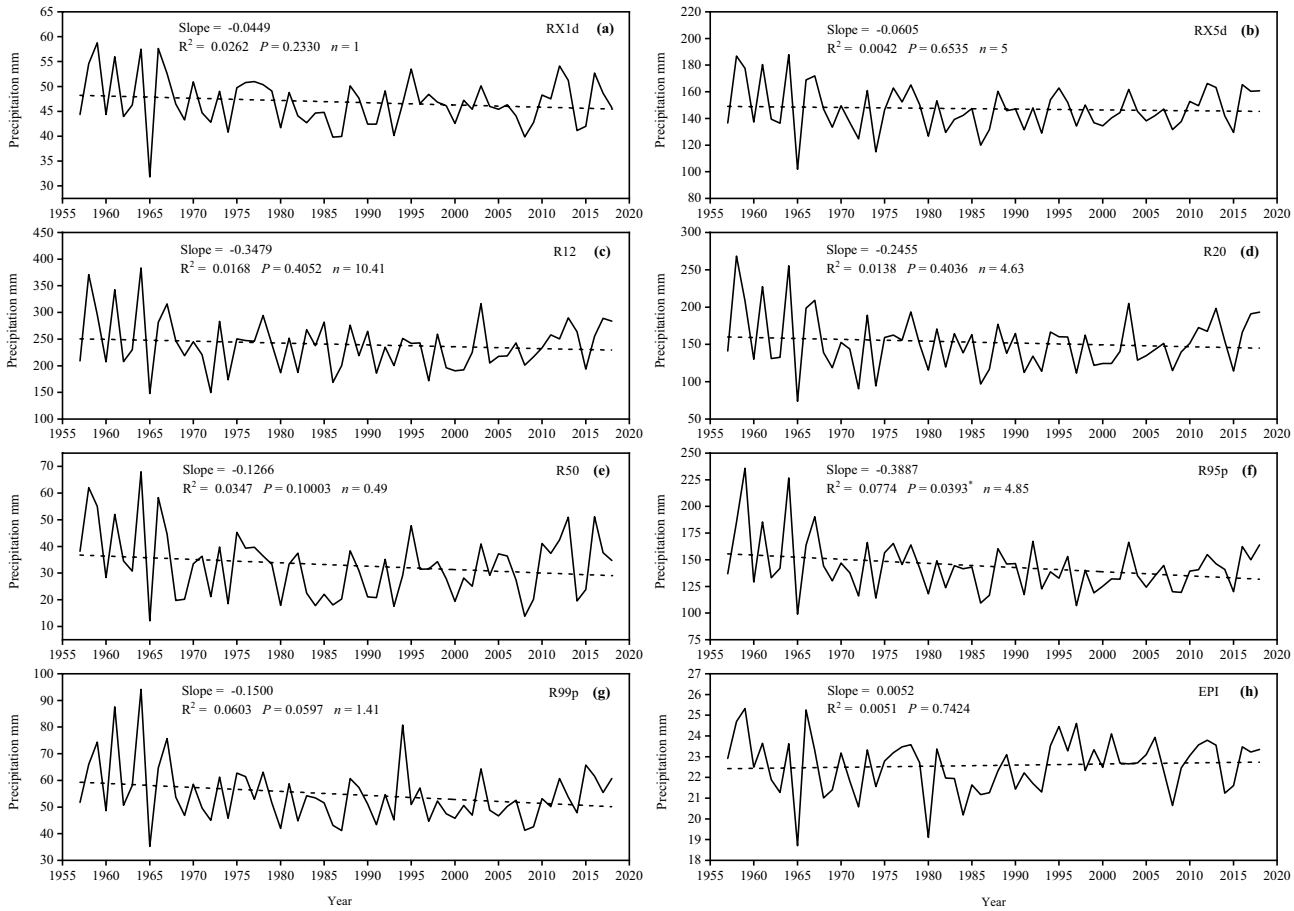

Fig. 2 The temporal variation in extreme precipitation indices on the Loess Plateau during 1957–2018. Notes: *n* denotes the average days of all meteorological stations in the selected extreme precipitation indices during 1957–2018 on the Loess Plateau

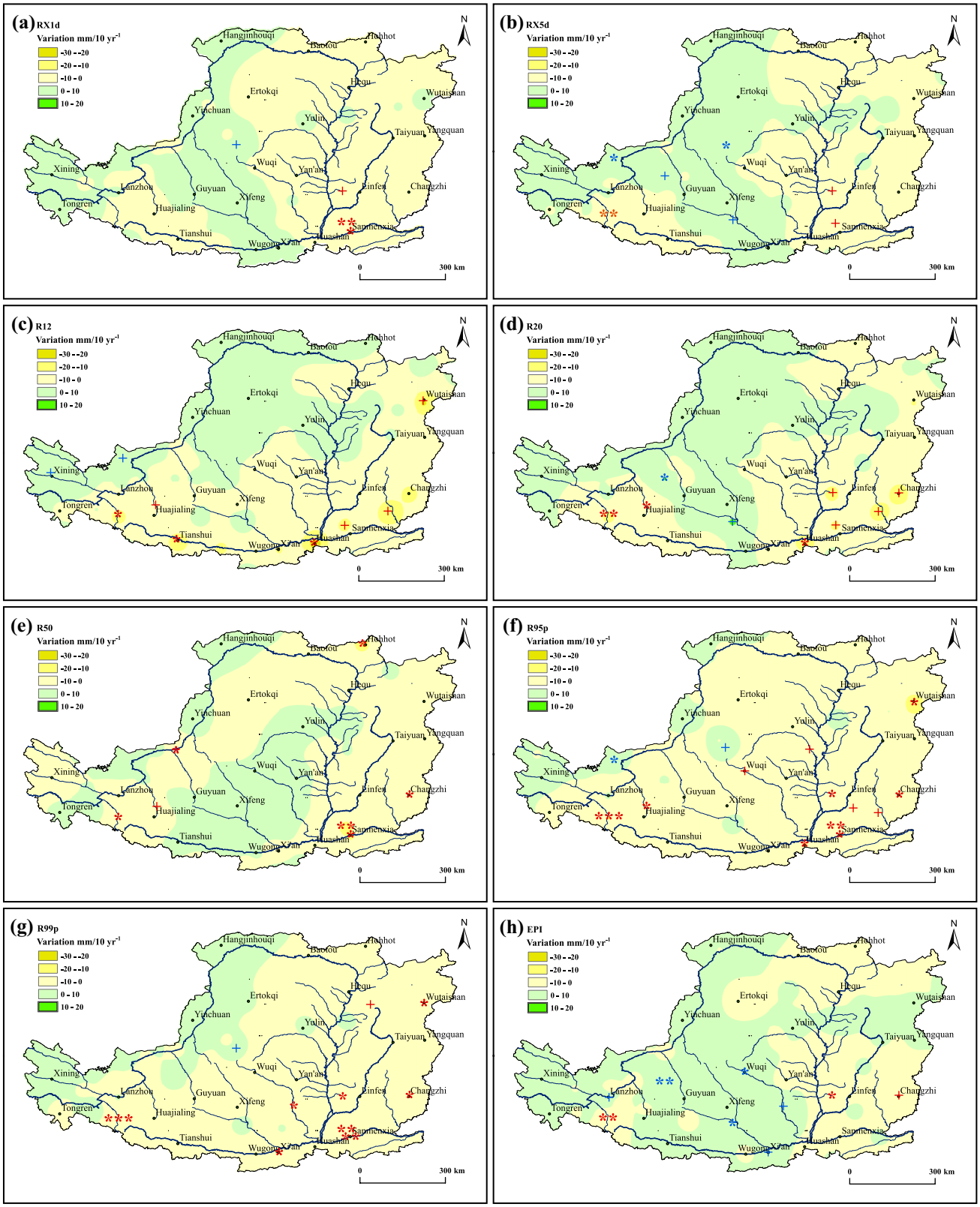

Fig. 3 The spatial variation in extreme precipitation indices across the Loess Plateau during 1957–2018. The red/blue symbols of "+, *, and **" indicate declining/increasing significance levels of 0.1, 0.05, and 0.01, respectively. The symbols in the other figures have the same meaning

indices of RX5d and R20 (Fig. 3b, d). We found that more than half of the Plateau had an ascending change in EPI (Fig. 3h). The areas with a descending change accounted for 64.3% (RX1d), 52.3% (RX5d), 59.2% (R12), 51.7% (R20), 65.3% (R50), 88.9% (R95p), 79% (R99p), and 41.8% (EPI) of the total area of the Loess Plateau, as shown in Fig. 3a–h, respectively.

Furthermore, decreasing changes in extreme precipitation events occurred in extensive areas of the eastern and southern parts of the Plateau. Further analysis indicated that a significant decreasing trend often appeared at a few meteorological stations, such as Yuncheng and Huashan, across the Loess Plateau. In contrast, increasing changes in all the extreme precipitation indices always occurred on the northwestern Loess Plateau (Fig. 3).

3.2 Variation in rainfall erosivity

The mean annual R over the Loess Plateau during 1957–2018 was 1159 MJ mm ha^{-1} h^{-1} $year^{-1}$, and it varied greatly from the southeast to northwest, ranging from 2921 to 251 MJ mm ha^{-1} h^{-1} $year^{-1}$ (Fig. 4a-l). R was distributed mainly from June to September, accounting for 85.2% of the annual totals; specifically, the R in July and August appeared to have a larger coefficient of variation (Fig. 4a-2).

The annual R over the Loess Plateau showed an insignificant decreasing change, with a declining rate of only − 3.1 6 MJ mm ha^{-1} h^{-1} $year^{-1}$ per 10 years. Consistent with the change pattern of the extreme precipitation events, the areas with increasing change were mainly on the northwestern Plateau, and the areas with decreasing change were mainly on the southeastern part, which covered 49.4% and 50.6% of the total area, respectively. Correspondingly, 32 stations exhibited positive changes, and only two of them showed statistically significant changes ($P < 0.1$). In contrast, 38 stations showed negative changes and only three were statistically significant ($P < 0.1$) (Fig. 4b).

The coefficient of variation (C_v) of annual R over the Loess Plateau showed an obvious regional difference, which showed a twofold decrease from the northwest to southeast. We also found that a higher C_v and a larger fluctuation of annual R were situated in the northwestern Plateau, which is the summer monsoon tail region (Fig. 4c).

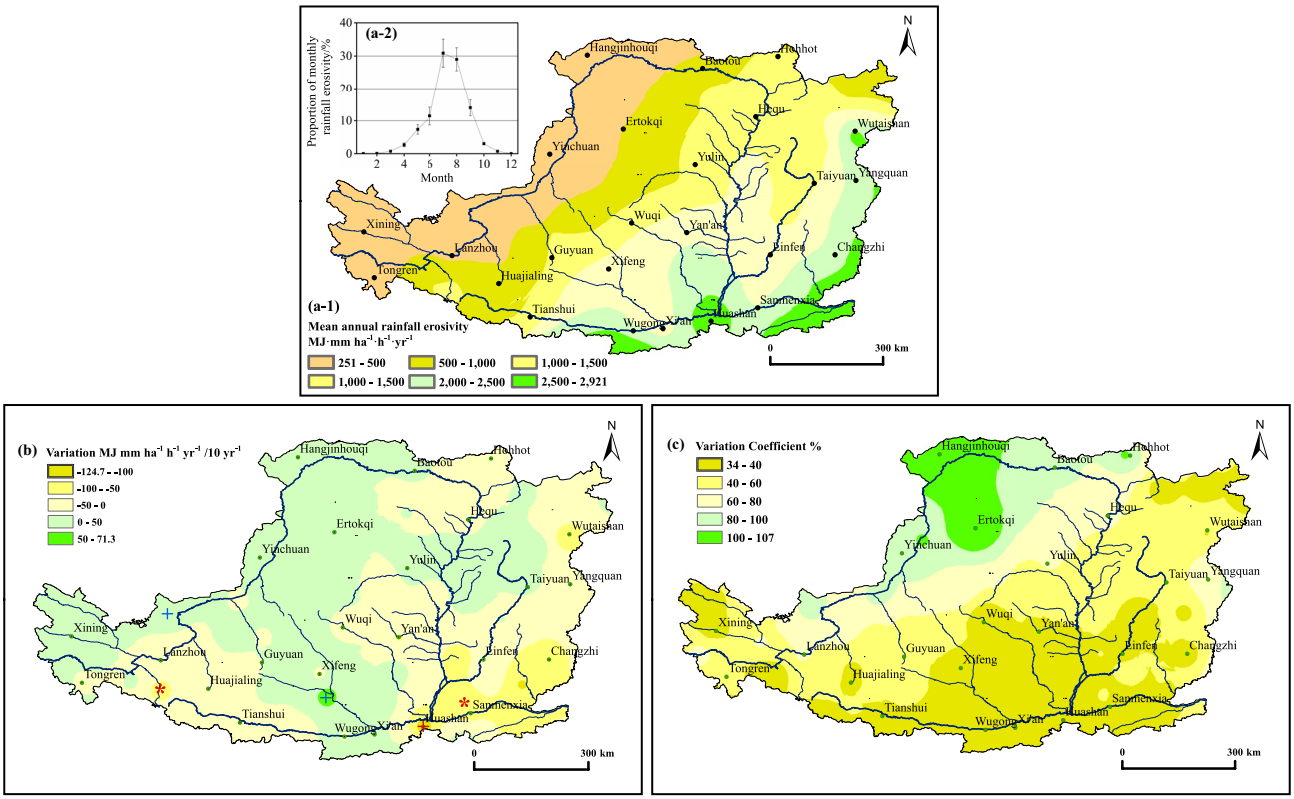

Fig. 4 Spatial distribution (**a**), variation (**b**), and C_v of annual rainfall erosivity (**c**) across the Loess Plateau from 1957 to 2018. The error bar in Fig. 4a-l represents the standard deviation of the proportion of monthly rainfall erosivity to the annual totals in six periods (namely, stage I from 1957 to 1970, stage II from 1971 to 1980, stage III from 1981 to 1990, stage IV from 1991 to 2000, stage V from 2001 to 2010, and stage VI from 2011 to 2018)

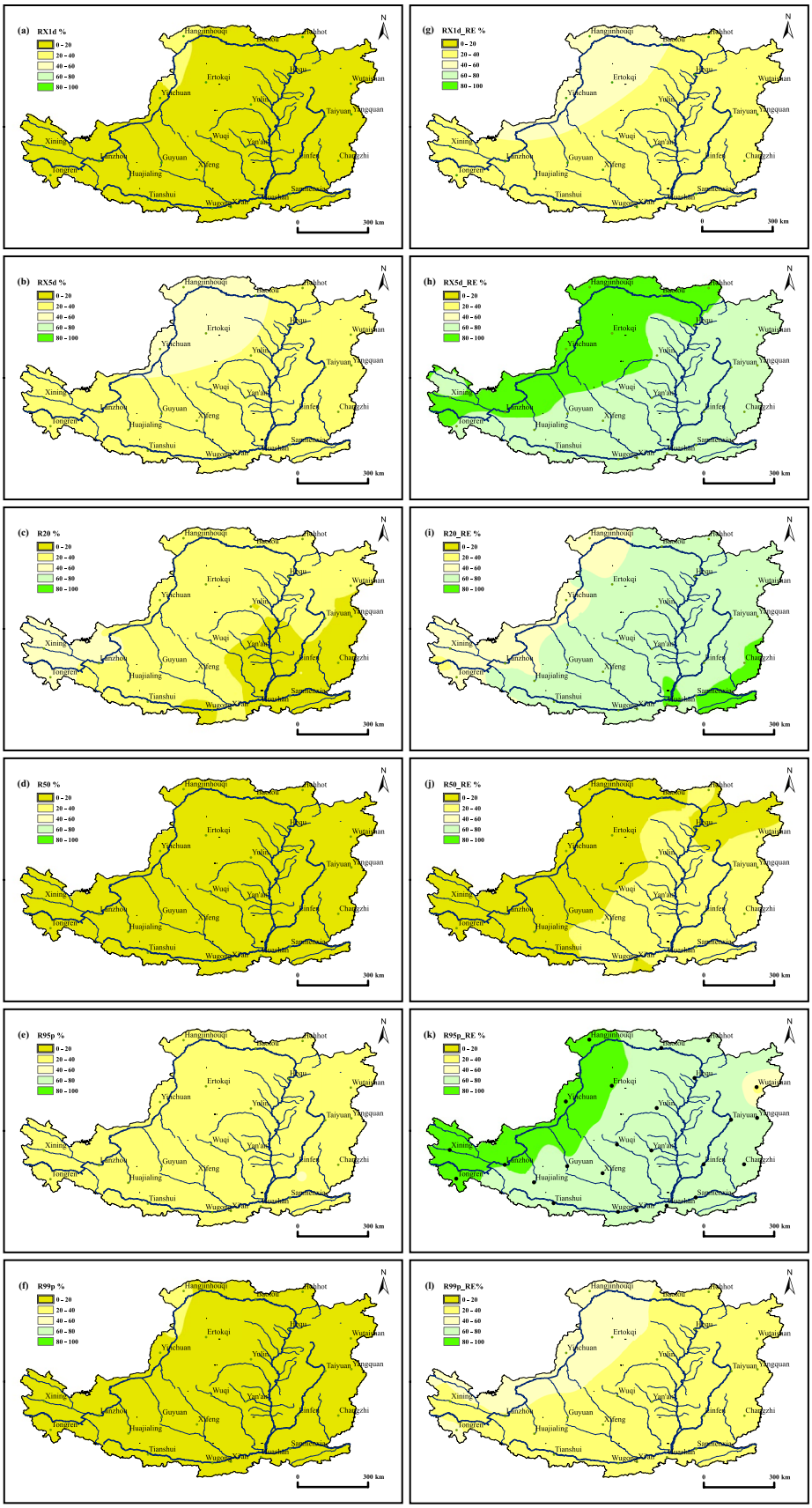

Fig. 5 Distribution of the proportion of precipitation derived from each index in the annual totals and the ratio of derived rainfall erosivity in the totals across the Loess Plateau during 1957–2018, respectively

3.3 Contribution of extreme precipitation events to rainfall erosivity

Figure 5 shows the mean annual distribution of the precipitation proportion derived from each of the indices in the annual total precipitation as well as the R proportion in the annual totals across the Loess Plateau over the past 62 years. The precipitation proportion from RX1d to the annual total precipitation was less than 20%, which nearly covered the entire Loess Plateau (Fig. 5a). Correspondingly, its ratio of R in most parts of the Plateau was between 20 and 40% (Fig. 5g). Overall, the precipitation proportions from RX5d and R20 were mostly between 30–50% and 30–40% across the Loess Plateau, respectively (Fig. 5b, c). However, their R ratios accounted for 60–90% and 60–80% on the Loess Plateau, respectively (Fig. 5h, i). We found that the Hangjinhouqi station lies in the arid area and northernmost part of the Loess Plateau, and its precipitation and R in RX5d occupied over 40% and 90% of the annual totals, respectively, which indicated that the annual precipitation and R in areas such as the station were more concentrated in a few precipitation events within a year. For R50, the precipitation proportion was less than 20%, but it explained 20–30% of R (Fig. 5d, j). The precipitation and associated R from R95p accounted for 30–40% and 60–90% of the annual total, respectively (Fig. 5e, k). For R99p, the proportion of precipitation and R was basically the same as that in RX1d (Fig. 5f, l).

We also found that the contribution to R increased to the northwest, especially for RX1d, RX5d, R95p, and R99p (Fig. 5g, h, k, and l), but the contribution to R increased closer to the southeast, especially for R20 and R50 (Fig. 5i, j).

As seen in Table 2, consistent with the changes detected in the EASMI, the precipitation and corresponding R derived from all seven indices showed a fast decreasing change from the first period to the second period and a slower increase from the second period to the third period. The changes could also be proven by the detected trend in Table 2. All seven indices showed an increasing change in the first period, while in the second period, four of seven indices showed an increase, and in the third period, all seven indices increased, with five of them increasing significantly. These results are consistent with those shown in Fig. 2. The proportion of precipitation derived from seven indices in the annual totals generally showed little change in the three periods, with a difference of less than 2%. For R, the proportion from seven indices also showed a similar change pattern with that for precipitation, in which the differences in three stages were less than 5%.

3.4 Effect of rainfall erosivity on sediment delivery

The R from R20 generally contributed 72.6% of the annual total over the whole Loess Plateau from 1957 to 2018, which was greater than that by other indices (Table 2). The annual R by R20, which occurred on approximately 5 days (Fig. 2), could better represent the effect of extreme precipitation events on soil erosion and sediment delivery on the Plateau. Therefore, R20 was used to investigate the effect of extreme events on annual sediment delivery.

Figure 6 shows a slight decrease in the annual R in the past 62 years by R20. Compared to the period of 1957–1970, the R by R20 decreased by 13.8%, 16.7%, 21.7%, and 17.9% in the 1970s, 1980s, 1990s, and 2000s, respectively. However, an increasing change of 0.4% was detected in the period of 2011–2018. The annual sediment delivery on the Loess Plateau showed a dramatic decreasing trend, from 18.12×10^8 t in 1957–1970 to 1.74×10^8 t

Table 2 The values and change of the EASMI and the values, change, and proportion (%) of extreme precipitation (P) and rainfall erosivity (R) at three periods on the Loess Plateau

Index	Period I (1957–1979)		Period II (1980–1999)		Period III (2000–2018)	
	Value/change		Value/change		Value/change	
EASMI	0.28/ − 0.024		− 0.33/ − 0.014		− 0.16/ − 0.011	
Index	P/change/proportion	R/change/proportion	P/change/proportion	R/change/proportion	P/change/proportion	R/change/proportion
RX1d	48.6/ − 0.13/10.7	361.4/ − 2.16/30.3	45.3/0.20/10.9	334.0/2.37/32.3	46.4/0.18/10.6	338.3/2.34/30.2
RX5d	150.9/ − 0.61/33.2	840.8/ − 6.97/70.1	142.1/0.62/34.1	751.5/3.96/70.3	148.0/1.10+/33.8	800.9/12.08/68.6
R12	252.6/ − 0.87/54.7	1213.4/ − 9.53/100	226.3/ − 0.11/53.7	1082.3/ − 0.21/100	239.1/4.6**/54.1	1184.1/24.12*/100
R20	162.0/ − 1.43/34.8	912.3/ − 10.51/74.2	140.5/ − 0.21/33.3	773.3/1.48/71.3	153.5/3.07*/34.6	855.1/19.9*/72.4
R50	37.7/ − 0.71/8.1	335.8/ − 4.82/27.0	27.8/0.54/6.7	257.4/0.92/23.6	32.4/0.74/7.3	288.2/7.10/23.7
R95p	154.6/ − 0.57/33.8	861.1/ − 7.56/71.5	134.8/ − 0.21/32.1	732.4/2.51/68.4	139.6/1.29+/31.7	783.5/11.33+/67.1
R99p	59.1/ − 0.23/12.9	425.0/ − 3.04/35.2	51.7/0.05/12.4	351.0/0.90/32.8	52.6/0.73*/12.0	366.7/4.36/31.4

P and R represent the extreme precipitation and corresponding rainfall erosivity of the selected indices, respectively. The change denotes the slope of the extreme precipitation and rainfall erosivity, with the unit denoting mm and MJ mm ha^{-1} h^{-1} $year^{-1}$, respectively

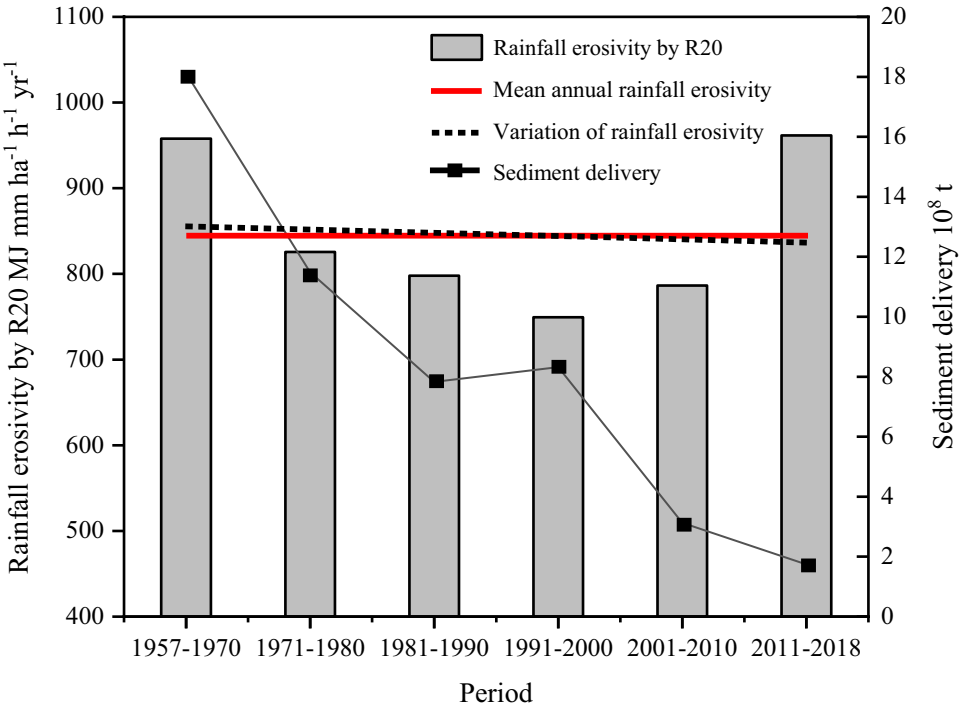

Fig. 6 Decadal variation in rainfall erosivity derived from R20 and sediment delivery over the Loess Plateau during 1957–2018. Note: The period division is consistent with Fig. 4

in 2011–2018. Compared with the period of 1957–1970, the sediment delivery during 1971–1980, 1981–1990, 1991–2000, 2001–2010, and 2011–2018 decreased by 36.6%, 56.8%, 54.1%, 82.7%, and 90.4%, respectively (Fig. 6). Figure 6 shows a significantly different change pattern between R and sediment yield over the past 62 years on the Loess Plateau.

Figure 7a shows two change points, 1979 and 1999, as detected by the double mass curve method, which were also proven by EASMI analysis (Li and Zeng 2002; Yin et al. 2019) and sediment research (Zhao et al. 2013; Wang et al. 2016; Zhang et al. 2018). The linear regressions illustrated in Fig. 7a and b show the significant differences in three periods divided by the change points. The regression

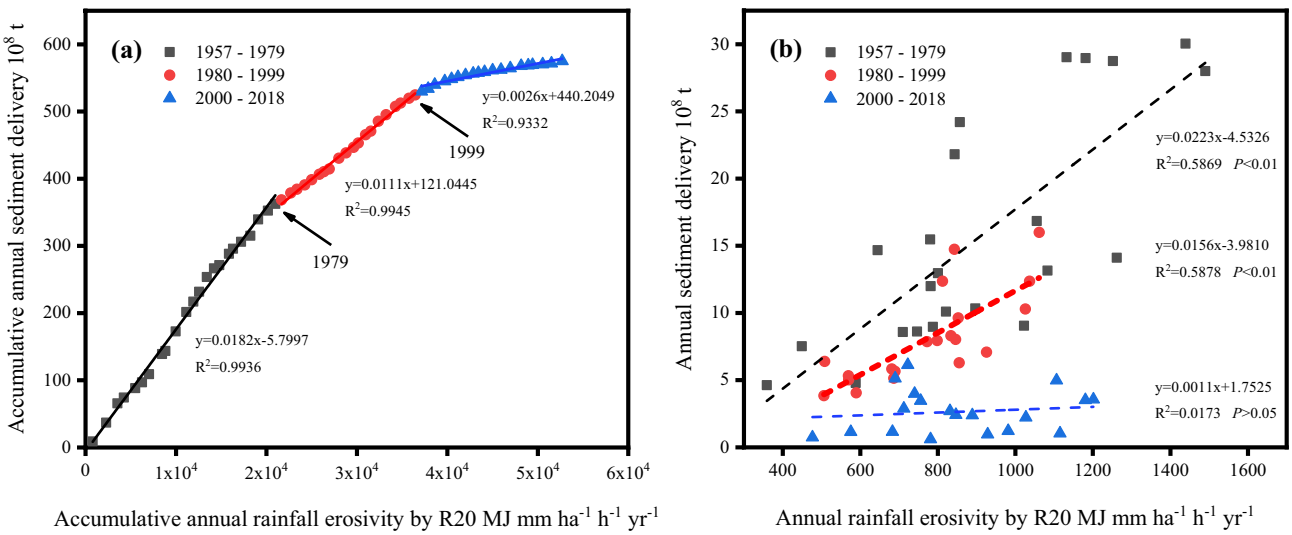

Fig. 7 Double mass curve analysis of annual rainfall erosivity derived from R20 and sediment delivery on the Loess Plateau (**a**); regression analysis of annual rainfall erosivity by R20 and annual sediment delivery at three stages (**b**). The symbols of the black box, red circle, and blue triangle represent the period prior to 1979, the period from 1980 to 1999, and the period after the "Grain for Green" project (GGP), respectively

Table 3 The impacts of climate change and human activities on sediment delivery in different periods on the Loess Plateau

Period	Average annual sediment delivery/10^8 t	Contribution rate by climate changes/%	Contribution rate by human activities/%
I (1957–1979)	15.8	-	-
II (1980–1999)	8.1	6.4	93.6
III (2000–2018)	2.7	−0.5	100.5

"-" means no data in the reference period of 1957–1979

coefficient showed a significant decrease in the three periods and the coefficients of determination in the former two periods passed the 0.01 significance test. However, there was no significant correlation between these two variables since 2000 (Fig. 7b). The sediment delivery per unit R decreased by 30.0% and 95.1% in the latter two periods, respectively.

Table 3 illustrates that in the latter two periods, the changes in R contributed just 6.4% and −0.5% to the reduction in sediment delivery on the Loess Plateau, respectively. This result implies that human activities such as the numerous soil conservation measures implemented since 1980 and the extensive vegetation restoration after 1999 strongly influenced the processes of soil erosion and sediment delivery in the region.

4 Discussion

4.1 Domination of extreme precipitation events to rainfall erosivity

The East Asian summer monsoon is proven to be the dominant natural factor that affects the spatiotemporal variation in precipitation on China's Loess Plateau, an arid and semi-arid area. The EASMI was reported to decrease by a rate of −0.124 per 10 years over the period from 1957 to 2018 (Li and Zeng 2002; Gu et al. 2016). These findings explained why extreme precipitation events by most of the indices over the Loess Plateau demonstrated a decreasing tendency from 1957 to 2018 (Fig. 2). The EPI showed a slight increasing change (Fig. 2), which was likely due to the unbalanced variation in the duration and the amounts of erosive precipitation in the region (Zhao et al. 2018). Additionally, R95p had a significant decreasing trend while the other indices showed only slight changes. This result was possibly due to the definition of the index itself and the randomness of extreme precipitation events especially on the Loess Plateau, an arid and semi-arid region. Furthermore, global climate change potentially resulted in the occurrence of these extreme precipitation events with inconsistent probabilities.

The spatiotemporal changes in annual extreme precipitation and associated R were generally consistent with the results of previous research (Li et al. 2010; Xin et al. 2011; Yang and Lu 2015; Sun et al. 2016; Zhao et al. 2018). Differences existed in the magnitude of decrease, which may be affected by the numbers of meteorological stations used in the research and their data series.

Table 2 shows that there was an obvious periodic pattern in extreme precipitation and associated R, which was basically consistent with the variation in the EASMI. In stage I from 1957 to 1979, extreme precipitation and the associated R showed a decreasing change, which was also demonstrated by Liu et al. (2018) and Zhao et al. (2018). However, in stage II from 1980 to 2000, we found that the changes in a few extreme precipitation events predominantly contributed to the increased R, especially in R20 and R95p. Their decreased precipitation along with the increased R indicated that these two extreme precipitation events experienced a stronger intensity in the period on the Loess Plateau, which was consistent with the report by Ren et al. (2016). In stage III from 2000 to 2018, all the indices, especially R12, R20, and R95p, experienced a significant increasing change in extreme precipitation amount and estimated R (Table 2). This result implied that the significant increasing tendency in the precipitation amount and R in R12 was very likely to be caused by that in R20 and R95p.

A remarkable regional difference was demonstrated in extreme precipitation and R in this study (Figs. 3 and 4). We found that extreme precipitation and R exhibited an upward change on the western margin of the Loess Plateau and a downward change in the central and eastern parts, which was supported by other reports (Yang and Lu 2015; Sun et al. 2016; Zhao et al. 2018; Soksamnang 2018).

The increased R in the western Plateau was likely due to the enhanced EPI and the associated extreme precipitation events for the intensified water cycle driven by global climate warming (Held and Soden 2006; IPCC 2007; Wang et al. 2012). Yin et al. (2019) found that summer precipitation on the eastern–central part of the Loess Plateau was strongly and positively correlated with the change in the EASMI. As shown in Figs. 2, 3, and 4, and Table 2, the weakening of the EASMI over the period was supposed to dominate the decreasing change in extreme precipitation and R in this region. The results were also confirmed by the research of Yang and Lu (2015) and Zhao et al. (2018).

4.2 Determination of extreme precipitation events to soil erosion

Soil erosion by rainfall on the Loess Plateau was highly concentrated in certain extreme precipitation events (Wang et al. 1996; Xin et al. 2011). The precipitation from R50, characterized by a relatively short duration and a high intensity, contributed approximately one-third of the annual R in most soil loss areas of the Plateau. The same situation existed in RX1d and R99p. For example, a heavy rainstorm with a return period of once-in-two-century occurred in Suide County of the northern Loess Plateau in 2017, which caused serious flooding and soil erosion leading to a catastrophic disaster for the local residents (Liu et al. 2017). Although the return period of R50 was less than once a year on the Loess Plateau, as shown in Fig. 2, but the land resources and ecological security of this region were greatly threatened (Wan et al. 2014; Chen et al. 2018). Figure 5 shows that RX5d, R20, and R99p equally contributed approximately 60–90% of the annual R, which means that soil erosion, particularly in the middle part of Loess Plateau, was caused mostly by these extreme rainfall events, all of which occurred on an average of 5 days per year.

Previous studies noted that soil loss was highly sensitive to precipitation types with short durations and very high intensities, which would result in severe land degradation on Chinese Loess Plateau (Zhou et al. 1992; Chen et al. 2018). The results suggested that we should attempt to eliminate the threat from a few extreme precipitation events by adopting appropriate soil conservation measures in the future.

4.3 Response of sediment delivery to rainfall erosivity changes

R is an important natural factor causing severe soil erosion and large sediment yield on China's Loess Plateau. It was found that the annual R over the Loess Plateau decreased slightly, while a sharp decrease in the annual sediment delivery occurred during the period of 1957–2018. The area of soil conservation measures was relatively limited prior to 1979 (Wang et al. 2016); Simultaneously, it was a period with a stronger effect of the summer monsoon. Extreme precipitation events often generated a high R in that period, which caused a large quantity of soil erosion and a mean annual sediment delivery up to 15.8×10^8 t to the Yellow River (Liu et al. 2019). From 1980 to 1999, the annual R exhibited a descending change, and the mean annual sediment delivery was reduced to 8.1×10^8 t (Liu et al. 2019). Many studies have demonstrated that the decreased sediment delivery in this period was primarily due to large-scale soil protection practices consisting of reservoirs, terraces, and check dams (Zhao et al. 2013; Liu et al. 2020).

From 2000 to 2018, increased R was observed, but sediment delivery was reduced to 2.7×10^8 t per year in the Yellow River (Zhang et al. 2008; Zhao et al. 2013; Liu et al. 2020). Wang et al. (2016) and Zhang et al. (2018) reported that extensive vegetation restoration due to the implementation of the "Grain for Green" project (GGP) since 1999 across the Loess Plateau potentially resulted in a sharp reduction in sediment yield. Our results support the recognition of the attenuated effects of extreme precipitation events on sediment yield (Fig. 7a, Table 3).

It was reported that the total vegetation coverage increased significantly from about 40% in 1982 to 76.8% in 2017 across the Loess Plateau (Li et al. 2019; Yang et al. 2020). Although there was no significant change in R over that time, the annual sediment delivery on the Loess Plateau sharply decreased from 15.8×10^8 t in 1957–1979 to 2.7×10^8 t in 2000–2018, respectively, which benefited from the continuous improvement of vegetation coverage (Liu et al. 2019). Beneficial human intervention exerted a positive effect on the soil erosion control and sediment delivery decreases in this region since 1980, especially after 1999 (Zhang et al. 2008; Wang et al. 2016; Liu et al. 2020).

It was also recognized that engineering measures and vegetation restoration have significantly changed the surface hydrological and erosion processes by aggravating the roughness on the ground over time (Li et al. 2009; IPCC 2013; Liu et al. 2017; Zhang et al. 2018). For instance, Liu et al. (2020) reported that soil conservation measures reduced surface runoff by alternating hydrodynamic conditions, which consequently triggered a reduction in sediment delivery in the Yellow River. Similarly, the mitigation of surface runoff and sediment yield by vegetation restoration was demonstrated by Quinton et al. (1997) and Sun et al. (2006). Moreover, this trend was proven by the slight sediment delivery modulus of 100 t km^{-2} $year^{-1}$ in Ziwuling Mountain area, which has a high vegetation coverage of 80%, on the Loess Plateau (Zheng 2006).

Although the above findings showed that soil conservation practices could fundamentally reduce soil detachment, appropriate measures for the floods and soil loss triggered by extreme precipitation events with a return period of once-in-10-year or once-in-one-century still need to be developed (Liu et al. 2017; Zhang et al. 2018; Zhao et al. 2018). In some areas with severe soil loss, the lack of litter layers and lower soil infiltration capacity under plantation vegetation result in an unstable ecological community structure and poor soil stress resistance; thus, these areas are easily prone to higher ecological environment vulnerability under extreme precipitation events (such as R20 and R95p with greater precipitation intensity) compared to natural forests (Wu et al. 2005; Li et al. 2011; Gu et al. 2019).

Therefore, it is very important to understand the spatiotemporal changes in extreme precipitation events and the associated R and develop suitable countermeasures to control corresponding soil erosion and sediment delivery for high-quality eco-tope development on Chinese Loess Plateau (Angulo-Martinez et al. 2009).

5 Conclusions

Understanding the spatiotemporal patterns of extreme precipitation and the associated R and the effects on soil erosion and sediment delivery is important in many parts of the world as well as on the Chinese Loess Plateau. We concluded that the annual R derived from R20 showed a slight decreasing change in the past 62 years. The R exhibited a staged descending change before 1999 but an ascending change since that year. Generally, all extreme precipitation indices showed a slight descending change in the past 62 years. Spatially, they showed a consistent changing pattern with a decreasing change in the southeast part of the Loess Plateau and an increasing change along the northwest edge. Three extreme precipitation indices, namely, RX5d, R20, and R95p, could explain 60–90% of the variation in total R. Compared with 1957–1979, the R from extreme precipitation events generated an attenuated contribution to the reduction of sediment delivery on the Loess Plateau in the periods of 1980 to 1999 and 2000 to 2018.

This study helps to understand the specific processes of ecohydrology and is useful for sustainable development in the region. The assessment methods and extreme precipitation indices have widespread applicability for other regions in the world.

Author contribution XX came up with the study idea, gathered, processed, and analyzed the most meteorological data, generated maps with ArcGIS, and wrote the original draft. LD and GJ did the statistical analysis. HT, HJ, and HL gave guidance in software operating. LX and LY provided partial basic data used in this study. GM guaranteed powerfully data analysis. YX and LB provided constructive suggestions for this article and did language polishing. ZX revised critically the draft, proposed good help to data analysis, and provided funding support. All the authors agreed with the final version of the manuscript, and revised the manuscript earnestly.

Declarations

Conflict of interest The authors declare no competing interests.

References

Angulo-Martinez M, Begueria S (2009) Estimating rainfall erosivity from daily rainfall records: a comparison among methods using data from the Ebro Basin (NE Spain). J Hydrol 379:111–121

Ballabio C, Borrelli P, Spinoni J, Meusburger K, Michaelides S, Beguería S, Klik A, Petan S, Janeček M, Olsen P, Aalto J, Lakatos M, Rymszewicz A, Dumitrescu A, Tadić MP, Diodato N, Kostalova J, Rousseva S, Panagos P (2017) Mapping monthly rainfall erosivity in Europe. Sci Total Environ 579:1298–1315

Cai QG (2001) Soil erosion and management on the Loess Plateau. J Geogr Sci 11(1):53–70

Chen H, Zhang XP, Abla M, Lü D, Yan R, Ren QF, Ren ZY, Yang YH, Zhao WH, Lin PF, Liu BY, Yang XH (2018) Effects of vegetation and rainfall types on surface runoff and soil erosion on steep slopes on the Loess Plateau, China. CATENA 170:141–149

Chen LD, Wei W, Fu BJ, Lu YH (2007) Soil and water conservation on the Loess Plateau in China: review and perspective. Prog Phys Geogr 31:389–403

Gu CJ, Mu XM, Gao P, Sun WY, Tatarko J, Tan XJ (2019) Influence of vegetation restoration on soil physical properties in the Loess Plateau, China. J Soils Sediments 19:716–728

Gu ZJ, Duan XW, Liu B, Hu JM, He JN (2016) The spatial distribution and temporal variation of rainfall erosivity in the Yunnan Plateau, Southwest China: 1960–2012. CATENA 145:291–300

Held IM, Soden BJ (2006) Robust responses of the hydrological cycle to global warming. J Clim 19(21):5686–5699

Hoyos N, Waylen PR, Jaramillo Á (2005) Seasonal and spatial patterns of erosivity in a tropical watershed of the Colombian Andes. J Hydrol 314(1–4):177–191

IPCC (2007) Summary for policymakers of climate change: The physical science basis. Contribution of working group into the fourth assessment report of the intergovernmental panel on climate change. Cambridge University Press, Cambridge UK

IPCC (2013) Climate change 2013: the physical science basis. Cambridge University Press, Cambridge

Kendall MG (1975) Rank correlation methods(4th ed.). Charles Griffin: London, UK

Li G, Sun SB, Han JC, Yan JW, Liu WB, Wei Y, Lu N, Sun YY (2019) Impacts of Chinese Grain for Green program and climate change on vegetation in the Loess Plateau during 1982–2015. Sci Total Environ 660:177–187

Li JP, Zeng QC (2002) A unified monsoon index. Geophys Res Lett 29(8):1274–1277

Li P, Zhao Z, Li ZB, XS (2011) Root distributions and drought resistance of plantation tree species on the Weibei Loess Plateau in China. Afr J Agric Res 6(21):4989–4997

Li Z, Liu WZ, Zhang XC, Zheng FL (2009) Impacts of land use change and climate variability on hydrology in an agricultural catchment on the Loess Plateau of China. J Hydrol 377(1–2):35–42

Li Z, Zheng FL, Liu WZ, Flanagan DC (2010) Spatial distribution and temporal trends of extreme temperature and precipitation events on the Loess Plateau of China during 1961–2007. Quat Int 226(1):92–100

Liu BY, Tang KL, Jiao JY, Ma XY, Zhang XP, Cao Q, Xiao PQ, Wei X, Fu SH, Miu CY, Li ZB, Zhao GJ (2019) Temporal and spatial atlas of water and sediment in the Yellow River. Science Press, Beijing, pp 3 (in Chinese)

Liu BY, Zhang KL, Xie Y (2002) An empirical soil loss equation. Proc of 12th ISCO, Beijing

Liu SY, Huang SZ, Huang Q, Xie YY, Leng GY, Luan JK, Song XY, Wei X, Li XY (2017) Identification of the non-stationarity of extreme precipitation events and correlations with large-scale ocean-atmospheric circulation patterns: a case study in the Wei River Basin, China. J Hydrol 548:184–195

Liu SY, Huang SZ, Xie YY, Leng GY, Huang Q, Wang L, Xue Q (2018) Spatial-temporal changes of rainfall erosivity in the Loess Plateau, China: changing patterns, causes and implications. CATENA 166:279–289

Liu XY, Li XY, Dang SZ (2016) Spatial pattern of precipitation change in the main sediment-yielding area of the Yellow River basin in recent years. J Hydraul Eng 47(4):463–472 (In Chinese)

Liu Y, Song HM, An ZS, Sun CF, Trouetf V, Cai QF, Liu RS, Leavittf SW, Song Y, Li Q, Fang CX, Zhou WJ, Yang YK, Jin Z, Wang YQ, Sun JY, Mu XM, Lei Y, Wang L, Li XX, Ren M, Cui LL, Zeng XL (2020) Recent anthropogenic curtailing of Yellow River runoff and sediment load is unprecedented over the past 500 y. PNAS 117(31):18251–18257

Mann HB (1945) Non-parametric tests against trend. Econometrica 13(3):245–259

Ministry of Water Resources of the People's Republic of China Announcement on Soil and Water Conservation in China. http://www.swcc.org.cn/gglm/2019/0820/38773.html, 2019–08–20
Panagos P, Ballabio C, Borrelli P, Meusburger K, Klik A, Rousseva S, Tadić MP, Michaelides S, Hrabalíková M, Olsen P, Aalto J, Lakatos M, Rymszewicz A, Dumitrescu A, Beguería S, Alewell C (2015) Rainfall erosivity in Europe. Sci Total Environ 511:801–814
Quinton JN, Edwards GM, Morgan RPC (1997) The influence of vegetation species and plant properties on runoff and soil erosion: results from a rainfall simulation study in south east Spain. Soil Use Manag 13(3):143–148
Ran Q, Su D, Li P, He Z (2012) Experimental study of the impact of rainfall characteristics on runoff generation and soil erosion. J Hydrol 424–425:99–111
Ren GY, Liu YJ, Sun XB, Zhang L, Ren YY, Ying XU, Zhang H, Zhan YJ, Wang T, Guo YJ (2016) Spatial and temporal patterns of precipitation variability over mainland China: III causes for recent trends. Advanc Water Sci 26(4):451–465 (In Chinese)
Renard KG, Foster R, Weesies G (1997) Predicting rainfall erosion by water: a guide to conservation planning with the Revised Universal Soil Loss Equation (RUSLE) In: USDA Agriculture Handbook 703, pp 1–367
Richardson CW, Foster GR, Wright DA (1983) Estimation of erosion index from daily rainfall amount. T ASAE 26(1):153–156
Searcy JK, Hardisoni CH, Langbein WB (1960) Double mass curves. Geological Survey Water Supply Paper 1541-B, US Geological Survey Washington DC
Sen PK (1968) Estimates of the regression coefficient based on Kendall's Tau. J Am Stat Assoc 63(324):1379–1389
Soksamnang KEO, He HM, Zhao HF, Jing SW (2018) Analysis of rainfall erosvity change and its impacts on soil erosion on the Loess Plateau over more than 50 years. Water Soil Conserv Res 25(2):1–7 (In Chinese)
Sun G, Zhou G, Zhang Z, Wei X, McNulty SG, Vose JM (2006) Potential water yield reduction due to forestation across China. J Hydrol 328:548–558
Sun WY, Mu XM, Song XY, Dan W, Cheng AF, Bing Q (2016) Changes in extreme temperature and precipitation events in the Loess Plateau (China) during 1960–2013 under global warming. Atmos Res 168(22):33–48
Tang KL, Xiong GS, Liang JY, Jing K (1993) Varieties of erosion and runoff sediment in Yellow River Basin. Chinese Sciences and Technique Press, Beijing, pp 4 (in Chinese)
Vallebona C, Pellegrino E, Frumento P, Bonari E (2015) Temporal trends in extreme rainfall intensity and erosivity in the Mediterranean region: a case study in southern Tuscany. Italy Clim Change 128(1–2):139–151
Wan L, Zhang XP, Ma Q, Zhang JJ, Ma TY, Sun YP (2014) Spatiotemporal characteristics of precipitation and extreme events on the Loess Plateau of China between 1957 and 2009. Hydrol Process 28(18):4971–4983
Wang L, D'Odorico P, Evans JP, Eldridge DJ, Mccabe MF, Caylor KK, King EG (2012) Dryland ecohydrology and climate change: critical issues and technical advances. Hydrol Earth Syst Sci 16(8):2585–2603
Wang S, Fu BJ, Sl P, Lv YH, Ciais P, Feng XM, Wang YF (2016) Reduced sediment transport in the Yellow River due to anthropogenic changes. Nat Geosi 9:38–41
Wang WZ, Jiao JY (1996) Sediment yield by rainfall erosion on the Loess Plateau and sediment transportation by Yellow River Science Press, Beijing, pp 169–170 (in Chinese)
Wei W, Chen LD, Fu BJ, Huang Z, Wu DP, Gui LD (2007) The effect of land uses and rainfall regimes on runoff and soil erosion in the semi-arid loess hilly area. China J Hydrol 335(3–4):247–258
Wischmeier WH, Smith DD (1978) Predicting rainfall erosion losses: a guide to conservation planning, in: Agriculture Handbook 537, US Department of Agriculture, Agricultural Research Service, Washington, D.C., 1978
Wu QX (2005) Mechanism of forest soil and water conservation and functional regulation technology. Science Press, Beijing, pp 7–8 (in Chinese)
Xie Y, Yin SQ, Liu BY, Nearing MA, Zhao Y (2016) Models for estimating daily rainfall erosivity in China. J Hydrol 535:547–558
Xin Z, Yu X, Li Q, Lu XX (2011) Spatiotemporal variation in rainfall erosivity on the Chinese Loess Plateau during the period 1956–2008. Reg Environ Change 11(1):149–159
Yang FB, Lu CH (2015) Spatiotemporal variation and trends in rainfall erosivity in China's dryland region during 1961–2012. CATENA 133:362–372
Yang XH, Zhang XP, Lv D, Yin SQ, Zhang MX, Zhu QGZ, Yu Q (2020) Remote sensing estimation of the soil erosion cover-management factor for China's Loess Plateau. Land Degrad Dev 1–14. https://doi.org/10.1002/ldr.3577
Yin YX, Chen HS, Zhai PM, Yu C, Ma HD (2019) Characteristics of summer extreme precipitation in the Huai River basin and their relationship with East Asia summer monsoon during 1960–2014. Int J Climatol 39(3):1555–1570
Yue S, Pilon P, Phinney B, Cavadias G (2002) The influence of autocorrelation on the ability to detect trend in hydrological series. Hydrol Process 16:1807–1829
Zhang XP, Lin PF, Chen H, Yan R, Zhang JJ, Yu YP, Liu EJ, Yang YH, Zhao WH, Lv D (2018) Understanding land use/cover change impacts on runoff and sediment load at flood events on the Loess Plateau. China Hydrol Process 32(4):576–589
Zhang XP, Zhang L, Zhao J, Rustomji P, Hairsine P (2008) Responses of streamflow to changes in climate and land use/cover in the Loess Plateau, China. Water Resour Res 44(7):W00A07. https://doi.org/10.1029/2007WR006711
Zhao GJ, Mu XM, Wen ZM, Wang F, Gao P (2013) Soil erosion, conservation, and eco-environment changes in the Loess Plateau of China. Land Degrad Dev 24(5):499–510
Zhao GJ, Zhai JQ, Tian P, Zhang LM, Mu XM, An ZF, Han MW (2018) Variations in extreme precipitation on the Loess Plateau using a high-resolution dataset and their linkages with atmospheric circulation indices. Theor Appl Climatol 133:1235–1247
Zheng FL (2006) Effect of vegetation changes on soil erosion on the Loess Plateau. Pedosphere 16(4):420–427
Zhou PH, Wang ZL (1992) A study on rainstorm causing soil erosion in the Loess Plateau. J Soil Water Conserv 6(3):1–5

Publisher's Note Springer Nature remains neutral with regard to jurisdictional claims in published maps and institutional affiliations.